Observation of Postsoliton Expansion Following Laser Propagation through an Underdense Plasma

Sarri, G., Singh, D. K., Davies, J. R., Fiuza, F., Lancaster, K. L., Clark, E. L., Hassan, S., Jiang, J., Kageiwa, N., Lopes, N., Rehman, A., Russo, C., Scott, R. H. H., Tanimoto, T., Najmudin, Z., Tanaka, K. A., Tatarakis, M., Borghesi, M., & Norreys, P. A. (2010). Observation of Postsoliton Expansion Following Laser Propagation through an Underdense Plasma. *Physical Review Letters*, *105*(17), [175007].
https://doi.org/10.1103/PhysRevLett.105.175007

Published in:
Physical Review Letters

Document Version:
Publisher's PDF, also known as Version of record

Observation of Postsoliton Expansion Following Laser Propagation through an Underdense Plasma

G. Sarri,[1] D. K. Singh,[2] J. R. Davies,[2] F. Fiuza,[2] K. L. Lancaster,[3] E. L. Clark,[4] S. Hassan,[4] J. Jiang,[2] N. Kageiwa,[5] N. Lopes,[2] A. Rehman,[6] C. Russo,[2] R. H. H. Scott,[3,6] T. Tanimoto,[5] Z. Najmudin,[6] K. A. Tanaka,[5] M. Tatarakis,[4] M. Borghesi,[1] and P. A. Norreys[3,6]

[1]*School of Mathematics and Physics, Queens University Belfast, BT7 1NN, United Kingdom*
[2]*GoLP, Instituto de Plasmas e Fusão Nuclear–Laboratório Associado, Instituto Superior Técnico, 1049-001 Lisbon, Portugal*
[3]*STFC Rutherford Appleton Laboratory, Didcot, OX11 0QX, United Kingdom*
[4]*Technological Educational Institute of Crete, GR 710 04 Greece*
[5]*Graduate School of Engineering, Osaka 565-0871, Japan*
[6]*Blackett Laboratory, Imperial College London, London SW7 2BZ, United Kingdom*

(Received 22 June 2010; published 22 October 2010)

The expansion of electromagnetic postsolitons emerging from the interaction of a 30 ps, 3×10^{18} W cm^{-2} laser pulse with an underdense deuterium plasma has been observed up to 100 ps after the pulse propagation, when large numbers of postsolitons were seen to remain in the plasma. The temporal evolution of the postsolitons has been accurately characterized with a high spatial and temporal resolution. The observed expansion is compared to analytical models and three-dimensional particle-in-cell results, revealing a polarization dependence of the postsoliton dynamics.

DOI: 10.1103/PhysRevLett.105.175007 PACS numbers: 52.35.Sb, 52.38.−r, 52.65.Rr, 52.70.Nc

The interaction of ultra-intense ($I \geq 10^{18}$ W cm^{-2}) laser pulses with plasmas provides a unique test bed for studying nonlinear, relativistic dynamics of macroscopic systems. In particular, nonlinear coherent modes can be excited in the wake of a laser pulse, providing one of the main vectors to transfer energy from the laser pulse to electromagnetic fields in the plasma and to fast particles. Among these modes, electromagnetic (EM) solitons [1–4] are one of the most important, since up to half of the laser energy density can be transferred to them [2]. During propagation through underdense plasma, a laser experiences a significant energy loss. As this energy loss is adiabatic, it is mostly translated into a redshift of the laser light [5]. In the case of initial plasma densities close to the critical density, this frequency decrease may eventually lead to the laser locally experiencing an overcritical plasma, thus becoming trapped in plasma cavities. On an electron time scale, these cavities preserve a radius of the order of the electron collisionless skin depth ($l_e = c/\omega_{pe}$, where ω_{pe} is the Langmuir plasma frequency) and are usually referred to as electromagnetic subcycle solitons [3]. These structures tend to be accelerated along plasma density gradients [6] and, therefore, are slowly propagating, if not steady in a homogeneous plasma. During this time, the ponderomotive repulsion of the trapped EM wave expels the electrons, leaving a positively charged core. On an ion time scale, the Coulomb repulsion of the ions left inside the cavity causes it to expand radially, and the soliton nature is lost: such late-time evolution of a soliton is thus commonly referred to as a *postsoliton* [7]. This mechanism resembles the Coulomb explosion of laser channels following relativistic self-focusing [8]. Postsoliton expansion has been studied analytically, using the so-called snowplow model [7,9,10] and the isolated spherical resonator model [11], and numerically, using particle-in-cell (PIC) codes [7]. A possible experimental indication of the presence of EM soliton structures in underdense plasmas has been reported in [12], and experimental observations of postsoliton structures were first reported in [13], where soliton remnants were observed in the dense region of a plasma resulting from the laser-driven explosion of a thin foil. Because of the nature of the plasma employed, clouds of bubblelike structures were detected, thus preventing the measurement of their temporal evolution.

In this Letter, we report the first experimental observation of well-isolated, single postsolitons. This allowed us, for the first time, to carry out temporally resolved measurements of postsoliton expansion and of the electric field distribution, validating previous numerical results and unveiling effects of laser polarization on postsoliton dynamics. The experimental results are compared to analytical and three-dimensional (3D) PIC simulation results. The experiment was carried out at the Rutherford Appleton Laboratory, employing the VULCAN Nd:glass laser [14]. A sketch of the setup is given in Fig. 1(a): 200 J of 1 μm laser light contained in a 30 ps full width half maximum pulse ["Int" in Fig. 1(a)] were focused to a peak intensity of 3×10^{18} W cm^{-2} at the edge of a supersonic deuterium gas jet with a backing pressure ranging from 1 to 100 bar. This resulted, once fully ionized, in an electron density of 10^{18}–10^{20} cm^{-3}, which is 0.001–0.1 times the nonrelativistic critical density n_c. The interaction was diagnosed via the proton radiography technique [13,15], which uses

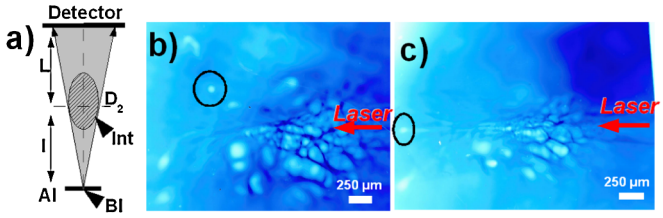

FIG. 1 (color online). (a) Top view of the experimental arrangement. (b)–(c) Radiographs of two different shots: outlined with dark circles are the density bubbles interpreted to be postsolitons.

a laser accelerated proton beam, produced by the interaction of a secondary laser pulse ($\tau \approx 1$ ps, $E \approx 100$ J, $I \geq 10^{19}$ W cm^{-2}, "Bl" in Fig. 1) with a 20 μm thick aluminum foil, as a charged particle probe. The virtual pointlike source [16] allowed imaging of the interaction area with a geometrical magnification $M \approx (l + L)/l \approx 6$, where $l \approx 6$ mm and $L \approx 3$ cm; see Fig. 1(a). The probe beam, after having passed through the gas jet, was recorded by a stack of radiochromic films (RCF) [17].

The data set comprised about 30 shots, in which both the deuterium density and the probe time were varied. Two typical proton radiographs obtained at a density of $0.1n_c$ are shown in Fig. 1. These images were obtained with protons of energy ≈ 4 MeV, 100 ps after the beginning of the interaction. As a rule of thumb, the electric fields are directed from the lighter blue regions (reduced proton flux) towards the darker blue regions (increased flux). In both images, a channel created by the laser pulse is visible in the low density region at the edge of the gas jet. In the dense region inside the gas jet, a strongly modulated deflection pattern is visible along the laser propagation axis. This scaly region highlights the presence of a cloud of bubbles that appear to be merged or overlying one another in this 2D projection, possibly surrounding the laser-driven channel. Such a region visually resembles the cloud of solitons that was experimentally and numerically observed in [13]. Ahead of and around this region, isolated bubblelike structures are visible (black circles in Fig. 1), most of them located at the end of laser filaments, as numerically predicted in [2]. These bubbles are associated with strong probe proton depletion with sharp edges. We note that these bubblelike structures, which we ascribe to postsolitons, were never observed at electron densities of $0.01n_c$ or less. Considering the isolated bubbles allows us to follow the fundamental properties of the temporal evolution of the postsolitons. Thanks to the multiframe capability of proton radiography [15], it is possible to follow the temporal evolution of these bubbles in the range 80–130 ps after the beginning of the interaction, i.e., 40–90 ps after the laser has left the gas jet, within the same laser shot. These bubbles were found to be effectively stationary in the laboratory reference frame and to expand, preserving a roughly circular shape (Fig. 2). Bulanov and Pegoraro [9] give analytical results for the expansion of 1D planar, 2D cylindrical, and 3D spherical postsolitons using the snowplow model. In 3D the diameter of the sphere is given by $d_0[3^{3/2}(t - t_0)/t_s]^{1/3}$ for $(t - t_0) \gg t_s$, where t_s is given by $\sqrt{2\pi d_0^2 n_i m_i/\langle E_0^2\rangle}$, d_0 is the initial diameter, n_i is the initial ion density, m_i is the ion mass, and $\langle E_0^2\rangle$ is the time average of the square of the initial oscillating electric field inside the postsoliton. We fitted the experimental results with this function, taking the initial diameter d_0 and the time of creation of the soliton t_0 as free parameters and $\langle E_0^2\rangle^{1/2} = 2 \times 10^{12}$ V m^{-1}, which is roughly the average value of 40% of the initial laser field. This choice is justified by recent theoretical results which show that almost 40% of the initial laser field is trapped within an EM soliton [2]. Even though this function was able to fit the experimental data (see Fig. 2), it implied a creation time at the end of, if not after, the laser pulse duration, which is not physically sensible. We therefore tried the cylindrical result $d_0[5(t - t_0)/t_s]^{2/5}$; this gave a more physically meaningful fit with a creation time close to the peak of the laser pulse in both cases. The initial diameters from the cylindrical fits are also more reasonable than those from the spherical fits, being ≈ 1 μm instead of ≈ 3 μm, since we have $c/\omega_{pe} \approx 0.53$ μm (see Fig. 2 for the fits). For $d_0 \approx 1$ μm, the time scale of the postsoliton expansion is $t_s \approx 68$ fs, justifying the assumption $t - t_0 \gg t_s$. Other bubbles in Fig. 1 and in different shots (not shown) have been found to expand in a similar fashion.

In order to understand why a 3D structure follows predictions for two rather than three dimensions, we carried out a 3D run with the PIC code OSIRIS [18]. We considered a linearly polarized laser pulse with a wavelength of 1 μm, Gaussian spatial and temporal profiles with FWHM of 6 μm and 1 ps, respectively, and a peak intensity of 3×10^{18} W cm^{-2} incident on a fully ionized deuterium

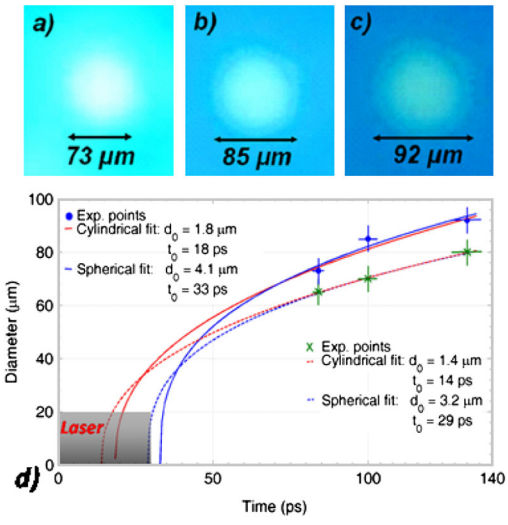

FIG. 2 (color online). Zoom in on the bubble structure outlined in Fig. 1 in different layers of the RCF stack corresponding to 84 ps (a), 100 ps (b), and 132 ps (c). (d) Bubble diameter as a function of time and fits using results from the snowplow model for cylindrical and spherical postsolitons.

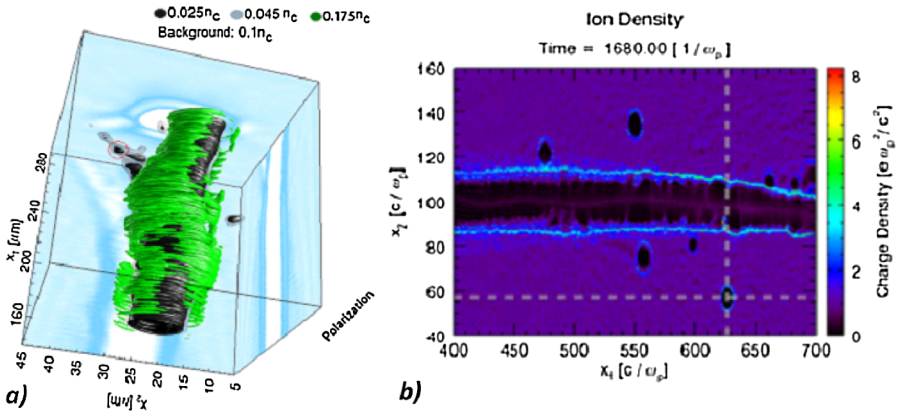

FIG. 3 (color online). (a) Isosurfaces of the ion density at 4.11 ps from 3D PIC modeling. (b) Ion density at 3 ps from 2D PIC modeling for *s*-polarized light. The dashed lines highlight the postsoliton from which the electric field distribution in Fig. 5 was taken.

plasma with a density of $0.1n_c$. The interaction was followed for 5 ps. The simulation box was $350 \times 50 \times 50$ μm, divided into 2.4×10^8 cells, each having two electrons and two deuterium ions, and the time step was 0.196 fs. The pulse duration and time considered are 30 times less than those in the experiment because of computational limitations. However, this was long enough for postsoliton formation to occur and to follow their expansion after the passage of the laser pulse. A number of longer 2D runs, with a larger number of particles per cell and a range of plasma densities, were also carried out for *s* polarization (laser electric field out of the plane) and *p* polarization (laser electric field in the plane). The ion density in Fig. 3(a) shows prolate spheroid postsolitons, with an aspect ratio of 5:3, lying outside the channel formed by the laser in the plane perpendicular to the laser electric field. In the 2D runs solitons were only ever formed for *s*-polarized light [see, for instance, Fig. 3(b)]. This dependence of soliton creation upon the laser polarization is in line with the PIC code results reported in [2]. The solitons were formed as the result of laser leakage into filaments that led to the creation of subchannels departing from the main channel [as visible in both Figs. 3(a) and 3(b)]. The postsolitons are elongated along the direction of the leaking radiation, so they would lead to a circular or slightly elliptical 2D projection in our experimental arrangement [Fig. 1(a)]

The nonspherical shape of the postsolitons at these early times gives a first indication as to why the spherical scaling may not apply. To determine the scaling of the postsoliton expansion with time, we measured the full width at one-quarter of the initial density of the postsoliton circled in Fig. 3(a) along X_2 (the smaller diameter) at various times, as given in Fig. 4. This definition of diameter was chosen because the electric field, which determines the shapes seen by the proton probing, showed a very high noise level. The precise definition used and the direction in which it is applied did not change the scaling, only the absolute values. We fitted these points with a power law (Fig. 4), which gave $t^{0.416}$, clearly in better agreement with the cylindrical scaling of $t^{2/5}$ than the spherical scaling of $t^{1/3}$, as the experimental data suggest. Following this, we fitted the diameter with the cylindrical scaling of $d_0[5(t - t_0)/t_s]^{2/5}$, taking t_0 and d_0 as free parameters and $\langle E_0^2 \rangle^{1/2} = 2.4 \times 10^{12}$ V m^{-1}, taken directly from the code results for this postsoliton, which is close to the value assumed in fitting the experimental results. This gave $t_0 = 3.5$ ps and $d_0 = 0.53$ μm, which gives $t_s = 31$ fs (Fig. 4). Again the assumption $t - t_0 \gg t_s$ is satisfied. The value of d_0 appears somewhat low ($d_0 < 2l_e$), but this is due to the way the diameter was determined, which clearly gave a value smaller than the outer edge of the postsoliton, which was difficult to determine unambiguously from the 3D results.

The snowplow model, upon which postsoliton theory relies, assumes total reflection of the trapped EM wave and ignores the outer plasma pressure. This is an adequate approximation only if the polarization of the trapped wave is parallel (*s* polarized) to the soliton overcritical walls ($R_s = 1$); *p*-polarized light will instead be partially absorbed [19], thus decreasing the reflectivity ($R_p < R_s$)

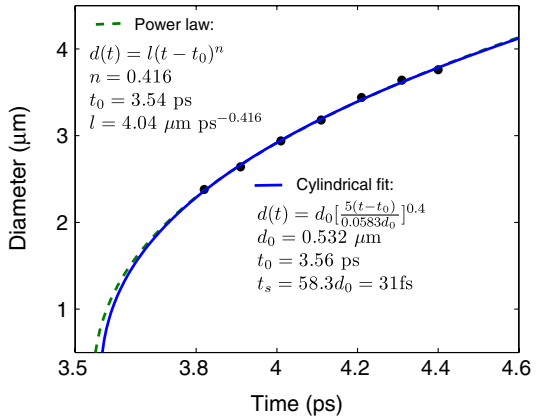

FIG. 4 (color online). Postsoliton diameter X_2 extracted from the 3D PIC results along with a power-law fit and a fit using the analytical result for a cylindrical postsoliton.

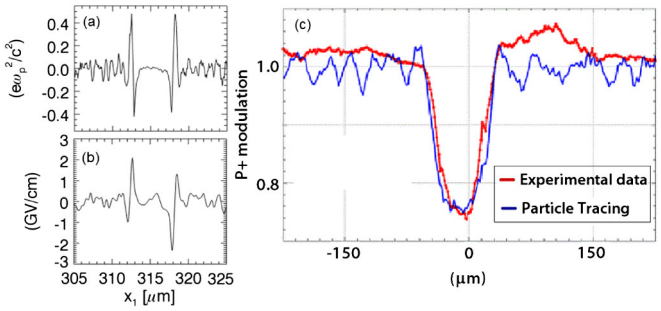

FIG. 5 (color online). (a) Cross-cut of the postsoliton charge density from 2D PIC modeling at 3 ps. (b) Corresponding electric field distribution. (c) Comparison between the modulation of the proton probing beam as directly obtained from the RCF (thick red line) and the modulation simulated via the PT code (thin blue line).

and increasing the pressure of the outer plasma. The radiation pressure considered in the snowplow model is $2I/c$, whereas it is $(1 + R_p)I/c - n_e K_B T_e < 2I/c$ for p-polarized light. Here n_e ($K_B T_e$) is the plasma density (temperature) at the edge of the postsoliton. One can envisage a scenario in which the trapped laser light will conserve, at least in a preliminary stage, its original polarization and the plasma cavity will have an approximately round shape. The trapped EM wave will have a reflectivity that depends upon the orientation of the walls to the wave polarization; s-polarized light will be totally reflected, whereas p-polarized light will be partially absorbed, thus inducing a smaller pressure on the soliton wall. An anisotropic expansion will thus occur, explaining why the postsoliton is seen to expand in a fashion that more closely resembles the cylindrical than the spherical snowplow model. This can also explain why p-polarized light is not able to excite stable EM solitons [2], as seen in our 2D simulations.

The electric field structure in the postsolitons was much clearer in the 2D PIC results, due to the much lower noise level (more particles could be used) and simpler geometry. Figure 5 shows a cross-cut through the electric field of the postsoliton, outlined by the dashed lines in Fig. 3(b), and the corresponding charge density. The electric field shows two sharp, bipolar peaks located at the edge of the postsoliton with a maximum amplitude of 2×10^{11} V m^{-1} at 3 ps after the beginning of the interaction. The electrostatic field is expected to scale as $E^2 \sim d^{-4}$; this is concluded on the basis that the ratio between the energy and the frequency of the trapped electric field is an adiabatic invariant during the postsoliton expansion [7]. Given a cylindrical scaling for the postsoliton diameter, we expect the amplitude of the electric field to decrease in time as $E \sim t^{-4/5}$. At 100 ps, the time of the measurements, the maximum amplitude of the electrostatic field should thus be $2 \times 10^{11}(100/3)^{-4/5} \approx 10^{10}$ V m^{-1}. This electric field deflects the probing protons in the experiment. In order to compare this result with the experimental ones, we used a particle tracing (PT) code that traces proton trajectories from a pointlike source through a given 3D electric field distribution up to the proton detector, giving a 2D proton density map at the detector plane. Therefore, the initial conditions for the PT code consisted of a uniform proton beam with an energy of 4 MeV crossing an electrostatic field with a spatial profile like the one in Fig. 5(b), with spherical symmetry and a maximum amplitude of 10^{10} V m^{-1}; the bipolar peaks of the electric field extended for 10 μm each, separated by a plateau region 60 μm long. A cross-cut of the code results and the experimental results is shown in Fig. 5; their good quantitative agreement further confirms the interpretation of the structures as postsolitons.

In summary, we report the experimental observation of isolated postsoliton structures in plasmas. For the first time, the postsoliton expansion has been resolved with high temporal and spatial resolution, giving information about its dynamics and electric field distribution. The postsoliton expansion is best described by the analytical prediction for cylindrically symmetric postsolitons. The 3D PIC code results show the same behavior and, along with the 2D results, indicate that this is due to polarization effects.

We acknowledge the contribution of the staff of the Central Laser Facility, and the OSIRIS consortium for the use of OSIRIS. This work was carried out under the auspices of the HiPER preparatory project and was supported by the UK Science and Technology Facilities Council.

[1] D. Farina and S. V. Bulanov, Phys. Rev. Lett. **86**, 5289 (2001).
[2] S. V. Bulanov *et al.*, Phys. Rev. Lett. **82**, 3440 (1999).
[3] T. Esirkepov *et al.*, Phys. Rev. Lett. **89**, 275002 (2002).
[4] G. Lehmann *et al.*, Phys. Plasmas **13**, 092302 (2006).
[5] S. V. Bulanov *et al.*, Phys. Fluids B **4**, 1935 (1992).
[6] Y. Sentoku *et al.*, Phys. Rev. Lett. **83**, 3434 (1999).
[7] N. M. Naumova *et al.*, Phys. Rev. Lett. **87**, 185004 (2001).
[8] A. G. Litvak, Sov. Phys. JETP **30**, 344 (1969); P. Sprangle *et al.*, IEEE Trans. Plasma Sci. **15**, 145 (1987).
[9] S. V. Bulanov and F. Pegoraro, Phys. Rev. E **65**, 066405 (2002).
[10] M. A. Leontovich and S. M. Osovets, At. Energ. **1**, 81 (1956) [J. Nucl. Energy **4**, 209 (1957)]; Ya. B. Zel'dovich and Yu. P. Raizer, *Physics of Shock Waves and High-Temperature Hydrodynamic Phenomena* (Academic Press, New York, 1967).
[11] L. D. Landau and L. M. Lifshits, *Electrodynamics of Continuous Media* (Pergamon, Oxford, 1984).
[12] L. M. Chen *et al.*, Phys. Plasmas **14**, 040703 (2007).
[13] M. Borghesi *et al.*, Phys. Rev. Lett. **88**, 135002 (2002).
[14] C. N. Danson *et al.*, J. Mod. Opt. **45**, 1653 (1998).
[15] G. Sarri *et al.*, New J. Phys. **12**, 045006 (2010).
[16] M. Borghesi *et al.*, Phys. Rev. Lett. **92**, 055003 (2004).
[17] J. F. Dempsey *et al.* Med. Phys. **27**, 2462 (2000).
[18] R. A. Fonseca, L. O. Silva, R. G. Hemker *et al.*, Lect. Notes Comput. Sci. **2331**, 342 (2002).
[19] S. C. Wilks and W. L. Kruer, IEEE J. Quantum Electron. **33**, 1954 (1997).